Nanoscale

COMMUNICATION

View Article Online
View Journal | View Issue

Cite this: *Nanoscale*, 2019, **11**, 4204

Received 3rd December 2018,
Accepted 14th February 2019

DOI: 10.1039/c8nr09734h

rsc.li/nanoscale

MnX (X = P, As) monolayers: a new type of two-dimensional intrinsic room temperature ferromagnetic half-metallic material with large magnetic anisotropy†

Bing Wang,‡[a] Yehui Zhang,‡[a] Liang Ma,[a] Qisheng Wu,[b] Yilv Guo,[a] Xiwen Zhang[c] and Jinlan Wang *[a,d]

Recent experimentally demonstrated intrinsic two-dimensional (2D) magnetism has sparked intense interest for advanced spintronic applications. However, the rather low Curie temperature and small magnetic anisotropic energy (MAE) greatly limit their application scope. Here, by using density functional theory calculations, we predict a series of stable 2D MnX (X = P, As, Sb) monolayers, among which MnP and MnAs monolayers exhibit intrinsic ferromagnetic (FM) ordering and considerably large MAEs of 166 and 281 μeV per Mn atom, respectively. More interestingly, the 2D MnP and MnAs monolayers exhibit highly desired half-metallicity with wide spin gaps of about 3 eV. Monte Carlo simulations suggest markedly high Curie temperatures of MnP and MnAs monolayers, ~495 K and 711 K, respectively. Besides, these monolayers are the lowest energy structures in the 2D search space with excellent dynamic and thermal stabilities. A viable experimental synthesis route is also proposed to produce MnX monolayers *via* the selective chemical etching method. The outstanding attributes of MnP and MnAs monolayers would substantially broaden the applicability of 2D magnetism for a wide range of applications.

Introduction

By exploiting the electron spin and its associated magnetic moment, spintronic devices are of particular interest in the field of quantum computing and next generation information technology.[1–3] Materials with specific spin order (magnetism) and diverse electronic properties, such as magnetic semiconductors and half-metals (behaving as a metal in one spin channel and as a semiconductor or insulator in the other spin channel), are highly desirable for advanced spintronic applications. However, the discovered magnetic semiconductors and half-metals are very limited and/or suffer from serious shortcomings, such as high cost and low Curie temperature (T_c). For example, intrinsic room-temperature magnetic semiconductors have never been observed experimentally despite decades of attempts. Inspired by the excellent attributes of atomically thin two-dimensional (2D) materials such as an ultra large specific surface area and novel electronic, mechanical and optical properties that may be absent in the bulk counterparts, numerous efforts have been devoted to achieving 2D magnetism. Only very recently, long-range 2D ferromagnetic (FM) order has been experimentally confirmed in semiconducting CrI_3 monolayers[4] and $Cr_2Ge_2Te_6$ bilayers.[5]

However, the presently demonstrated 2D magnetic semiconductors still show rather low T_c (45 K for the CrI_3 monolayer and 30 K for the $Cr_2Ge_2Te_6$ bilayer), far from practical room temperature spintronic applications. On the other hand, one may be aware that FM metal thin films usually exhibit a much higher T_c due to the strong exchange interaction driven by charge carriers,[6] such as ScCl monolayers for 185 K,[7] MnB monolayers for 345 K,[8] MoN_2 monolayers for 420 K,[9] Fe_2Si nanosheets for 780 K,[10] Co_2Se_3 monolayers for 600 K,[11] and very recently observed Fe_3GeTe_2 monolayers for 130 K.[12] In view of these observations, the 2D half-metal becomes a potential alternative option as the T_c of the 2D half-metal is expected to be much higher than that of 2D magnetic semiconductors because of the abundant charge carriers in the 2D half-metal. In addition, the half-metal can intrinsically provide 100% spin-polarized current for highly efficient spintronics devices.[13] Nevertheless, although a number of potential nanomaterials (mainly nanowires,[14–16] transition metal compounds,[17–19] and metal-free systems[20–22]) have been theoretically proposed, 2D intrinsic room-temperature half-metals are rarely reported.

According to the Mermin–Wagner theorem,[23] no long-range magnetic ordering at finite temperatures would exist in 2D

[a]*School of Physics, Southeast University, Nanjing 211189, China. E-mail: jlwang@seu.edu.cn*
[b]*Department of Chemistry and Chemical Biology, the University of New Mexico, USA*
[c]*School of Mechanism Engineering & School of Physics, Southeast University, Nanjing 211189, China*
[d]*Synergetic Innovation Center for Quantum Effects and Applications (SICQEA), Hunan Normal University Changsha, Hunan 410081, P. R. China*

†Electronic supplementary information (ESI) available. See DOI: 10.1039/c8nr09734h

‡These authors contributed equally to this work.

systems within the *isotropic* Heisenberg model with continuous spin symmetries. Thus, magnetocrystalline anisotropy (MCA) is fundamentally critical to give rise to long-range magnetic ordering in 2D materials by breaking the continuous spin symmetry of the Hamiltonian.[24] Besides, MCA can also help to preserve the direction of magnetic moments from heat fluctuation. The MCA can be scaled by the magnetic anisotropy energy (MAE). The larger the MAE, the better the resistance of magnetic ordering against the heat fluctuation. In recent years, enhancing the MAE becomes the most effective strategy to prevent the heat fluctuation to disturb the magnetic ordering. Considering the importance of magnetic anisotropy, it is of fundamental interest to discover new 2D FM materials with a sizable MAE.

In this work, we predict an emerging class of 2D intrinsic FM materials (MnP and MnAs monolayers) with significant magnetocrystalline anisotropy and large magnetic moments. More strikingly, these two FM monolayers are half-metallic with wide half-metallic gaps and exhibit ultra-high Curie temperatures (495 K for the MnP monolayer and 711 K for the MnAs monolayer). Besides, they possess thermal and dynamic stabilities up to 800 K and are the global minima in 2D space. A feasible experimental fabrication route is also proposed.

Computational method

Spin-polarized density functional theory (DFT) calculations were performed with the Perdew–Burke–Ernzerhof (PBE) functional in the generalized gradient approximation (GGA)[25] as implemented in the Vienna *ab initio* simulation package (VASP).[26] The plane-wave cutoff energy was set to 500 eV. The lattice geometries and atomic positions were fully relaxed until force and the energy were converged to 0.01 eV $Å^{-1}$ and 10^{-6} eV, respectively. To appropriately account for the strongly correlated electrons, the GGA+U method[27,28] (U_{eff} = 4.0 eV) was used to treat the d orbital of the Mn atoms and it was used throughout the paper. A detailed test on U_{eff} can be found in Table S1 and Fig. S1.† The HSE06 hybrid functional was employed to obtain the accurate electronic band structures and verify the GGA+U method.[29] For the MAE calculation, the spin–orbit coupling (SOC) was included. Phonon dispersions were calculated by density functional perturbation theory embedded in the PHONOPY codes.[30] *Ab initio* molecular dynamics (AIMD) simulations were conducted in the NVT ensemble up to 10 ps with a time step of 1.0 fs, during which the temperature was controlled by using a Nosé–Hoover thermostat.[31]

Results and discussion

MnX (X = P, As, Sb)[32–38] are ferromagnetic materials with high T_c, *e.g.*, ~320 K for MnAs[36] and ~600 K for MnSb.[39] Whether the high T_c nature of MnX can be succeeded in the atomically thin 2D form is still an open question. Actually, to our knowledge, their 2D counterparts have never been reported in the literature. Herein, we propose the concept of 2D MnX monolayer sheets. The optimized lattice structures of MnX monolayers are displayed in Fig. 1a, which are isostructural to the synthesized AFM FeSe monolayer.[40] MnX monolayers with various magnetic ordering, including FM and four antiferromagnetic (AFM) states, are considered and the corresponding spin configurations and parameters are presented in Fig. S2a–d and Tables S2 and S3 of the ESI.† It is found that the ground states of both MnP and MnAs monolayers have FM ordering with large magnetic moments, where the magnetism mainly stems from the Mn atoms while the P/As atoms hold small opposite spin moments as shown in the spin density distribution (Fig. 1b and c). However, the MnSb monolayer has an AFM ground state, which is not our target material in the present work. Electron localization functions (ELFs) show that the valence electron distributions are fully concentrated at the P/As atoms in the MnP/MnAs monolayer while they are absent around Mn atoms (Fig. S3†), reflecting the ionic bonding nature in MnX monolayers. Such an ionic bonding nature is further evidenced by Bader charge analysis, in which apparent electron transfer from Mn atoms to X atoms is observed (Table S1†).

The electronic properties of MnP and MnAs monolayers are then investigated. The spin-polarized band structures of the FM phases of the MnP and MnAs monolayers are shown in Fig. 1d and f, respectively. Notably, the spin-up bands cross the Fermi Level while the spin-down channel acts as a semiconductor for both sheets, indicating that they are intrinsic half-metallicity. The half-metallicity is further confirmed by

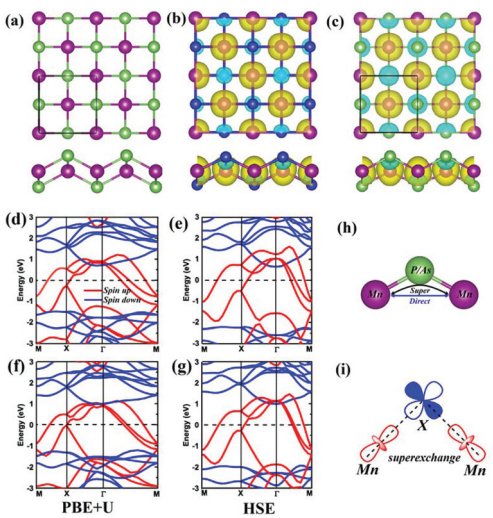

Fig. 1 (a) Top and side views of a 2D MnX sheet. The spin polarization distribution with the iso-surface of 0.05 e $Å^{-3}$ for MnP (b) and MnAs (c), respectively. The yellow and blue colors indicate the net spin-up and spin-down polarization, respectively, and the spin polarization is mainly on the Mn sites. Band structures of 2D MnP (d, e) and MnAs (f, g) monolayers in spin-up (red lines) and spin-down (blue lines) channels. (d, f) are calculated by using the PBE+U method and (e, g) are calculated by using the HSE06 method. (h, i) Illustrations of direct-exchange and super-exchange mechanisms.

the more accurate HSE06 hybrid functional as shown in Fig. 1e and g, respectively. In order to preserve the half-metallicity at room temperature, the band gap of the semiconducting channel should be wide enough to prevent the thermally excited spin–flip transition. The band gaps on the spin-down channel are 2.86 and 2.92 eV for the MnP and MnAs at the HSE06 level, respectively, which are wide enough to prevent spin leakage. The corresponding atom-projected and orbital-projected densities of states (Fig. S5†) indicate that the major magnetism in these 2D crystals is contributed by the Mn atom, more specifically the Mn 3d orbitals near the Fermi level. The half-metallicity with wide spin gaps makes 2D MnP and MnAs monolayers ideal candidates for miniaturized spintronic materials.

The ferromagnetic coupling of the MnP and MnAs monolayers can be well understood by the competition between the direct exchange and super-exchange of Mn atoms mediated through the P/As atom (Fig. 1h). According to the Goodenough–Kanamori–Anderson (GKA) rules,[41–43] the super-exchange interaction usually favors ferromagnetic ordering, especially for systems with a cation–anion–cation bond angle of 90°. The FM superexchange dominates the total exchange interaction in MnP and MnAs monolayers due to the ignored direct-exchange interaction with much large Mn–Mn distances (Table S1 and Fig. S5†). Since the Mn–P/As–Mn bond angles are close to 90°, the P/As-p orbital is nearly orthogonal to the Mn-d orbital, which leads to a negligible overlap integral S (Fig. 1i). According to the Heitler–London model,[44] the exchange integral J can be written as $J \approx 2k + 4\beta S$, where k, β, and S are the potential exchange, hopping integral, and overlap integral, respectively. Due to the near zero overlap integral S, J is reduced to $2k$, which is positive according to Hund's rule. As a result, MnP and MnAs monolayers both favor the ferromagnetic ordering.

Both MnX monolayers exhibit the integer magnetic moment of $8\mu_B$ per unit cell. The local magnetic moment on the Mn atom is about $4\mu_B$. A freestanding Mn atom has a valence electronic configuration of $4s^2 3d^5$ and Bader charge analysis indicates that the Mn atom loses electrons to the P/As atom (Table S1†). The unpaired d electrons contribute magnetism in MnP and MnAs monolayers. According to Hund's rules and the Pauli Exclusion Principle, the left four unpaired d electrons result in the magnetic moment of $4\mu_B$ per Mn atom.

The aforementioned magnetic anisotropy energy (MAE) is very important to determine the thermal stability of magnetic ordering. For 2D FM crystals, MCA mainly originates from the spin–orbit coupling (SOC) interaction.[45,46] Heavy elements are more preferred because their strong SOC effect can lead to a large MAE. SOC calculations are therefore performed on 2D MnP and MnAs monolayers to obtain relative stabilities along the (100), (010), (111), and (001) directions as summarized in Table 1. Clearly, the easy axes of these crystals are along the out-of-plane (001) direction, similar to those of the 2D CrI_3 monolayer[4] and Fe_3GeTe_2 monolayer.[12] The MAE of the MnP (MnAs) monolayer along the (001) direction is lower in energy than that along the (100), (010), and (111) directions by 166 (280), 164 (281), and 122 (216) μeV per Mn atom, respectively, which are significantly larger than the experimental values of the Fe monolayer/Rh (111) (80 μeV) and Co monolayer/Pt (111) (100 μeV) systems.[47] The larger MAE in MnAs originates from the stronger SOC since the As atom is heavier than the P atom. To our knowledge, such large MAEs have rarely been observed in 2D magnetic materials.

Table 1 Magnetic anisotropy energies (μeV) per Mn atom of different directions against the (001) direction, magnetic moment (M, μ_B) per Mn atom, anisotropy constant K (μeV), and Curie temperatures T_c (K) for 2D MnP and MnAs crystals

System	E(100)–E(001)	E(010)–E(001)	E(111)–E(001)	K_1	K_2	M	T_c
MnP	166	164	122	0.204	0.037	4	495
MnAs	280	281	216	0.380	0.103	4	711

Based on the uniaxial tetragonal symmetry of 2D MnP and MnAs monolayers, the angular dependence of the magnetocrystalline anisotropy energy can be described using the following equation:[48]

$$\mathrm{MAE}\ (\theta) = K_1 \sin^2\theta + K_2 \sin^4\theta, \quad (1)$$

where K_1 and K_2 are the anisotropy constants and θ is the azimuthal angle of rotation. If $K_1 > 0$ and predominates, the preferred magnetization direction will be along an out-of-plane easy axis (z-axis), whereas $K_1 < 0$ suggests that it will be perpendicular to the z-axis. Our calculated MAEs display a good fit of eqn (1) as presented in Fig. 2a and b, which depicts the angular dependence of MAE for MnP and MnAs monolayers in the xy, yz, and xz planes. It clearly shows that the MAE strongly

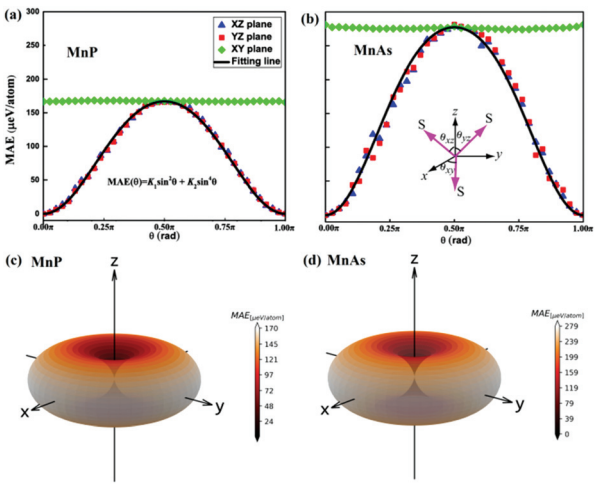

Fig. 2 Angular dependence of the MAE of MnP and MnAs monolayers with the direction of magnetization lying on three different planes (a, b) and the whole space (c, d). The inset illustrates that the spin vector S on the xy, yz, and xz planes is rotated with an angle θ about the x, y, and z axes, respectively. Lighter coloration and radial distance indicate the increase in MAE.

depends on the direction of magnetization in the *yz* and *xz* planes, whereas the energy is isotropic (straight line) in the *xy* plane. The MAE reaches a maximum value of 166 (281) μeV per Mn for MnP (MnAs) at $\theta_{xz} = \theta_{yz} = \pi/2$, suggesting that these monolayers belong to the family of 2D Ising magnets. Fitting from the angular dependence of MAE, the K_1 values of 2D MnP and MnAs monolayers are both positive and predominant (Table 1), which agrees with the fact that they both exhibit a single easy axis. The corresponding MAEs through the whole space are also plotted in Fig. 2c and d. Clearly, the MAEs show a strong dependence on the *yz* and *xz* planes and a much weaker dependence on the *xy* plane. This confirms again the strong magnetic anisotropy in these monolayers. The observed large MAEs will be sufficient to stabilize FM ordering against heat fluctuation at a certain temperature.

Generally, the T_c of the magnetic material positively correlates with its MAE. The calculated large MAE implies that high T_c can be anticipated in 2D MnP and MnAs monolayers. To quantitatively estimate the T_c of 2D MnP and MnAs monolayers, we performed Monte Carlo simulations based on the Heisenberg model. The Hamiltonian is defined as

$$H = -\sum_{ij} J_1 S_i S_j - \sum_{ik} J_2 S_i S_k - A S_i^Z S_i^Z,$$

where J_1 and J_2 are the first and second nearest-neighboring exchange parameters (Fig. S6†), respectively (more details are given in the ESI†). Using the energy difference of different magnetic configurations, the exchange parameters J_1 and J_2 of the MnP (MnAs) monolayer are calculated to be 3.3 meV (6 meV) and 13.9 meV (12.9 meV), respectively. The simulated magnetic moment and magnetic susceptibility of MnP and MnAs with respect to temperature (Fig. 3a and b) show that the T_c values of MnP and MnAs monolayers are about 495 and 711 K, respectively. These values are significantly higher than those ever reported, *e.g.*, CrI_3 monolayers (45 K),[4] Fe_3GeTe_2 monolayers (130 K),[12] and $Cr_2Ge_2Te_6$ bilayers (30 K).[5] Some other values are also shown in Fig. 3c for comparison. Note that our calculated T_c for the CrI_3 monolayer is ~43 K, which is in excellent agreement with the experimental measurement of 45 K. Moreover, the estimated T_c based on Ising models can be as high as 745 K and 1050 K for MnP and MnAs monolayers (Fig. S7†), respectively.

The stabilities of 2D crystals are crucial for experimental fabrication and practical applications. We conducted *ab initio* molecular dynamics simulations to evaluate the thermal stability of MnP and MnAs monolayers at temperatures of 300 K (Fig. S4†) and 800 K (Fig. 4a and b), respectively. The corresponding fluctuations of the total potential energies oscillate in a very narrow range, showing the good thermal stability of these monolayers. The absence of imaginary modes establishes the dynamic stability of MnP and MnAs monolayers as well (Fig. 4c and d).

Although MnP and MnAs monolayers have good stability, this only means that they are local minimal structures on the potential energy surface. Note that the global minimum structures are more likely to be realized in experiment. Are the above discussed MnX monolayers the global minima in 2D space? To address this issue, we carried out a global search for the low-energy stable structures based on the particle swarm optimization (PSO) scheme algorithm as implemented in the

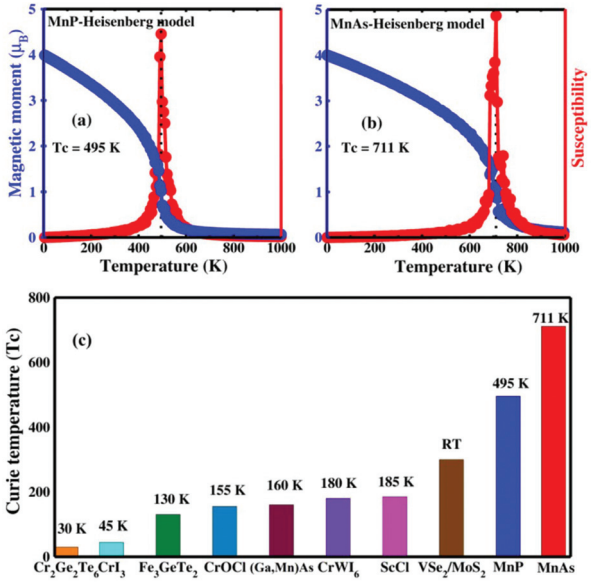

Fig. 3 On-site magnetic moment of Mn atoms and magnetic susceptibility *versus* temperature in MnP (a) and MnAs (b) monolayers based on the Heisenberg model. (c) Curie temperature in comparison with 2D $Cr_2Ge_2Te_6$,[5] CrI_3,[4] Fe_3GeTe_2,[12] CrOCl,[49] $CrWI_6$,[50] ScCl,[7] VSe_2/MoS_2,[51] and the most-studied dilute magnetic (Ga, Mn)As.[52] RT represents room temperature.

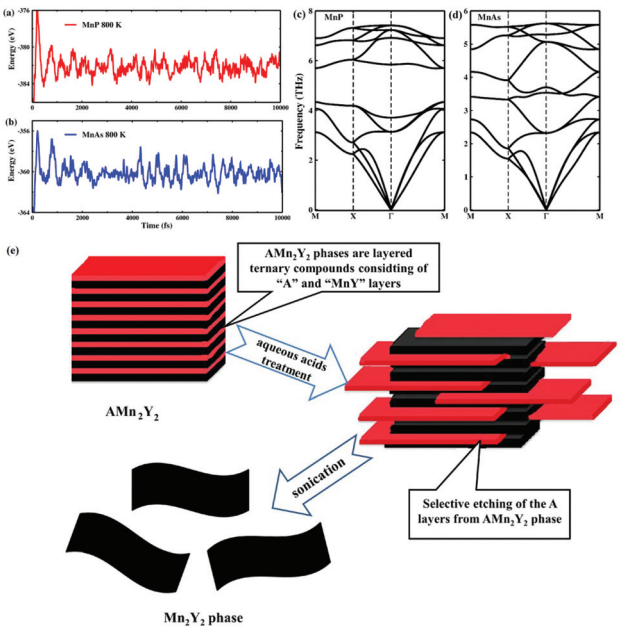

Fig. 4 Evolution of the total energy of MnP (a) and MnAs (b) with a temperature of 800 K. Phonon dispersion of the MnP monolayer (c) and MnAs monolayer (d). Schematic describing the synthesis process of MnY from the AMn_2Y_2 phase (e).

CALYPSO code[53] (more details are given in the ESI†). As shown in Fig. S8,† our proposed MnP/MnAs monolayers have the lowest energy in our global PSO search.

Considering their good thermal and dynamic stabilities and global minima, it is natural to wonder how to synthesize these 2D MnP and MnAs nanosheets in experiment. Selective chemical etching has been widely used to convert 3D MXenes phases to 2D phases, such as Ti_2AlC to Ti_2C[54] and MoAlB to MoB.[55] The key for such a method is the relatively weak interlayer interaction in 3D structures.[56,57] The ternary layered compounds AMn_2Y_2 (A = K, Ca, Sr, Ba, Y = P, As) have already been synthesized,[58–61] in which the MnY layer and alkaline A earth layer are alternatively stacked in the *c*-axis (Fig. S9†). Taking $BaMn_2Y_2$ as the example, the exfoliation energies of MnP and MnAs monolayers from the $BaMn_2Y_2$ are only 0.066 and 0.074 eV $Å^{-2}$ (Table S4†), respectively, which are even lower than those of most MXenes (0.086–0.205 eV $Å^{-2}$).[56] Besides, the elastic constant C_{11} of bulk $BaMn_2Y_2$ is much larger than C_{33} (Table S4†), showing that the stiffness of the overall chemical bonds along the *ab* direction is stronger than that along the *c* direction. Therefore, the combination of the A atom layer and MnY layer is relatively weak, and the corresponding MnP and MnAs sheets could be produced by selective chemical etching of the A atomic layer. A possible synthesis route for 2D MnY from 3D AMn_2Y_2 is therefore proposed in Fig. 4e.

In summary, we have reported two experimentally viable 2D intrinsic ferromagnetic materials, MnP and MnAs monolayers, which expose appreciable out-of-plane anisotropy with sizable magnetic anisotropy energy. More importantly, these 2D MnP and MnAs sheets exhibit remarkable half-metallicity with high Curie temperature (495 K for the MnP monolayer and 711 K for the MnAs monolayer). Besides, they are the lowest energy structures in our 2D search space and show excellent dynamic and thermal stabilities above room temperature. Moreover, the excellent ferromagnetism and half-metallicity can be well preserved in few-layer MnP and MnAs, *e.g.*, the bilayer case (Fig. S10 and S11†). Our discovery of intrinsic room temperature ferromagnetic materials of 2D MnP and MnAs crystals with half-metallicity provides new candidates for exploring fundamental physics and opens up new possibilities for spintronic applications at the nanoscale.

Conflicts of interest

There are no conflicts to declare.

Acknowledgements

This work was supported by the National Key Research and Development Program of China (2017YFA0204800), the Natural Science Funds of China (21525311, 21773027), the Jiangsu 333 project (BRA2016353), the Scientific Research Foundation of Graduate School of Southeast University (YBJJ1773), and the Fundamental Research Funds for the Central Universities of China. The authors acknowledge the computational resources at the SEU and National Supercomputing Center in Tianjin.

References

1 X. Li and J. Yang, *Natl. Sci. Rev.*, 2016, **3**, 365–381.
2 B. Huang, G. Clark, D. R. Klein, D. MacNeill, E. Navarro-Moratalla, K. L. Seyler, N. Wilson, M. A. McGuire, D. H. Cobden, D. Xiao, W. Yao, P. Jarillo-Herrero and X. Xu, *Nat. Nanotechnol.*, 2018, **13**, 544.
3 Y. P. Feng, L. Shen, M. Yang, A. Wang, M. Zeng, Q. Wu, S. Chintalapati and C. R. Chang, *Wiley Interdiscip. Rev.: Comput. Mol. Sci.*, 2017, **7**, e1313.
4 B. Huang, G. Clark, E. Navarro-Moratalla, D. R. Klein, R. Cheng, K. L. Seyler, D. Zhong, E. Schmidgall, M. A. McGuire, D. H. Cobden, W. Yao, D. Xiao, P. Jarillo-Herrero and X. Xu, *Nature*, 2017, **546**, 270–273.
5 C. Gong, L. Li, Z. Li, H. Ji, A. Stern, Y. Xia, T. Cao, W. Bao, C. Wang, Y. Wang, Z. Q. Qiu, R. J. Cava, S. G. Louie, J. Xia and X. Zhang, *Nature*, 2017, **546**, 265–269.
6 C. Zener, *Phys. Rev.*, 1951, **82**, 403–405.
7 B. Wang, Q. Wu, Y. Zhang, Y. Guo, X. Zhang, Q. Zhou, S. Dong and J. Wang, *Nanoscale Horiz.*, 2018, **3**, 551–555.
8 Z. Jiang, P. Wang, X. Jiang and J. Zhao, *Nanoscale Horiz.*, 2018, **3**, 335.
9 F. Wu, C. Huang, H. Wu, C. Lee, K. Deng, E. Kan and P. Jena, *Nano Lett.*, 2015, **15**, 8277–8281.
10 Y. Sun, Z. Zhuo, X. Wu and J. Yang, *Nano Lett.*, 2017, **17**, 2771–2777.
11 P. Lv, G. Tang, C. Yang, J. Deng, Y. Liu, X. Wang and J. Hong, *2D Mater.*, 2018, **5**, 045026.
12 Z. Fei, B. Huang, P. Malinowski, W. Wang, T. Song, J. Sanchez, W. Yao, D. Xiao, X. Zhu, A. F. May, W. Wu, D. H. Cobden, J. H. Chu and X. Xu, *Nat. Mater.*, 2018, **17**, 778–782.
13 X. Li and J. Yang, *Wiley Interdiscip. Rev.: Comput. Mol. Sci.*, 2017, **7**, e1314.
14 X. Li, H. Lv, J. Dai, L. Ma, X. C. Zeng, X. Wu and J. Yang, *J. Am. Chem. Soc.*, 2017, **139**, 6290–6293.
15 Y. Wan, Y. Sun, X. Wu and J. Yang, *J. Phys. Chem. C*, 2018, **122**, 989–994.
16 T. Zhang, L. Zhu and G. Chen, *J. Mater. Chem. C*, 2016, **4**, 10209–10214.
17 Q. Wu, Y. Zhang, Q. Zhou, J. Wang and X. C. Zeng, *J. Phys. Chem. Lett.*, 2018, **9**, 4260–4266.
18 Y. Zhao, L. Lin, Q. Zhou, Y. Li, S. Yuan, Q. Chen, S. Dong and J. Wang, *Nano Lett.*, 2018, **18**, 2943–2949.
19 Y. Tong, Y. Guo, K. Mu, H. Shan, J. Dai, Y. Liu, Z. Sun, A. Zhao, X. C. Zeng, C. Wu and Y. Xie, *Adv. Mater.*, 2017, **29**, 1703132.
20 Y. Nie, M. Rahman, P. Liu, A. Sidike, Q. Xia and G.-h. Guo, *Phys. Rev. B*, 2017, **96**, 075401.
21 D. Mpoutas and L. Tsetseris, *Phys. Chem. Chem. Phys.*, 2017, **19**, 26743–26748.

22 Z. Liu, J. Liu and J. Zhao, *Nano Res.*, 2017, **10**, 1972–1979.
23 N. D. Mermin and H. Wagner, *Phys. Rev. Lett.*, 1966, **17**, 1133–1136.
24 N. C. Frey, H. Kumar, B. Anasori, Y. Gogotsi and V. B. Shenoy, *ACS Nano*, 2018, **12**, 6319–6325.
25 J. P. Perdew, K. Burke and M. Ernzerhof, *Phys. Rev. Lett.*, 1996, **77**, 3865–3868.
26 G. Kresse and J. Furthmüller, *Phys. Rev. B: Condens. Matter Mater. Phys.*, 1996, **54**, 11169–11186.
27 L. Wang, T. Maxisch and G. Ceder, *Phys. Rev. B: Condens. Matter Mater. Phys.*, 2006, **73**, 195107.
28 P. Larson, W. R. L. Lambrecht, A. Chantis and M. van Schilfgaarde, *Phys. Rev. B: Condens. Matter Mater. Phys.*, 2007, **75**, 045114.
29 J. Heyd, G. E. Scuseria and M. Ernzerhof, *J. Chem. Phys.*, 2003, **118**, 8207–8215.
30 S. Baroni, S. de Gironcoli, A. Dal Corso and P. Giannozzi, *Rev. Mod. Phys.*, 2001, **73**, 515–562.
31 G. J. Martyna, M. L. Klein and M. Tuckerman, Nosé–Hoover chains, *J. Chem. Phys.*, 1992, **97**, 2635–2643.
32 I. Rungger and S. Sanvito, *Phys. Rev. B: Condens. Matter Mater. Phys.*, 2006, **74**, 024429.
33 A. Janotti, S.-H. Wei and L. Bellaiche, *Appl. Phys. Lett.*, 2003, **82**, 766–768.
34 I. Galanakis and P. Mavropoulos, *Phys. Rev. B: Condens. Matter Mater. Phys.*, 2003, **67**, 2635–2643.
35 A. K. Das, C. Pampuch, A. Ney, T. Hesjedal, L. Daweritz, R. Koch and K. H. Ploog, *Phys. Rev. Lett.*, 2003, **91**, 087203.
36 S. H. Chun, S. J. Potashnik, K. C. Ku, J. J. Berry, P. Schiffer and N. Samarth, *Appl. Phys. Lett.*, 2001, **78**, 2530–2532.
37 S. Sanvito and N. A. Hill, *Phys. Rev. B*, 2000, **62**, 15553–15560.
38 A. Continenza, S. Picozzi, W. T. Geng and A. J. Freeman, *Phys. Rev. B: Condens. Matter Mater. Phys.*, 2001, **64**, 085204.
39 K. Ono, J. Okabayashi, M. Mizuguchi, M. Oshima, A. Fujimori and H. Akinaga, Fabrication, *J. Appl. Phys.*, 2002, **91**, 8088.
40 Q. Y. Wang, Z. Li, W. H. Zhang, Z. C. Zhang, J. S. Zhang, W. Li, H. Ding, Y. B. Ou, P. Deng, K. Chang, J. Wen, C. L. Song, K. He, J. F. Jia, S. H. Ji, Y. Y. Wang, L. L. Wang, X. Chen, X. C. Ma and Q. K. Xue, *Chin. Phys. Lett.*, 2012, **29**, 037402.
41 J. Kanamori, *J. Appl. Phys.*, 1960, **31**, S14–S23.
42 P. W. Anderson, *Phys. Rev.*, 1959, **115**, 2–13.
43 J. B. Goodenough, *Phys. Rev.*, 1955, **100**, 564–573.
44 J.-P. Launay and M. Verdaguer, *Electrons in molecules: from basic principles to molecular electronics*, Oxford University Press, 2013.
45 J. Hu, P. Wang, J. Zhao and R. Wu, *Adv. Phys.: X*, 2018, **3**, 1432415.
46 H. L. Zhuang, P. R. C. Kent and R. G. Hennig, *Phys. Rev. B*, 2016, **93**, 134407.
47 A. Lehnert, S. Dennler, P. Błoński, S. Rusponi, M. Etzkorn, G. Moulas, P. Bencok, P. Gambardella, H. Brune and J. Hafner, *Phys. Rev. B: Condens. Matter Mater. Phys.*, 2010, **82**, 094409.
48 K. H. J. Buschow and F. R. d. Boer, *Physics of magnetism and magnetic materials*, Kluwer Academic/Plenum Publishers, New York, 2003, vol. 92.
49 N. Miao, B. Xu, L. Zhu, J. Zhou and Z. Sun, *J. Am. Chem. Soc.*, 2018, **140**, 2417–2420.
50 C. Huang, J. Feng, F. Wu, D. Ahmed, B. Huang, H. Xiang, K. Deng and E. Kan, *J. Am. Chem. Soc.*, 2018, **140**, 11519–11525.
51 M. Bonilla, S. Kolekar, Y. Ma, H. C. Diaz, V. Kalappattil, R. Das, T. Eggers, H. R. Gutierrez, M. H. Phan and M. Batzill, *Nat. Nanotechnol.*, 2018, **13**, 289.
52 K. Sato, L. Bergqvist, J. Kudrnovský, P. H. Dederichs, O. Eriksson, I. Turek, B. Sanyal, G. Bouzerar, H. Katayama-Yoshida, V. A. Dinh, T. Fukushima, H. Kizaki and R. Zeller, *Rev. Mod. Phys.*, 2010, **82**, 1633–1690.
53 Y. Wang, J. Lv, L. Zhu and Y. Ma, *Phys. Rev. B: Condens. Matter Mater. Phys.*, 2010, **82**, 094116.
54 M. Naguib, V. N. Mochalin, M. W. Barsoum and Y. Gogotsi, *Adv. Mater.*, 2014, **26**, 992–1005.
55 L. T. Alameda, P. Moradifar, Z. P. Metzger, N. Alem and R. E. Schaak, *J. Am. Chem. Soc.*, 2018, **140**, 8833–8840.
56 M. Khazaei, A. Ranjbar, K. Esfarjani, D. Bogdanovski, R. Dronskowski and S. Yunoki, *Phys. Chem. Chem. Phys.*, 2018, **20**, 8579–8592.
57 Z. Guo, L. Zhu, J. Zhou and Z. Sun, *RSC Adv.*, 2015, **5**, 25403–25408.
58 J. An, A. S. Sefat, D. J. Singh and M.-H. Du, *Phys. Rev. B: Condens. Matter Mater. Phys.*, 2009, **79**, 075120.
59 Y. Singh, M. A. Green, Q. Huang, A. Kreyssig, R. J. McQueeney, D. C. Johnston and A. I. Goldman, *Phys. Rev. B: Condens. Matter Mater. Phys.*, 2009, **80**, 100403(R).
60 S. W. Lovesey and D. D. Khalyavin, *Phys. Rev. B*, 2018, **98**, 054434.
61 J. Zeng, S. Qin, C. Le and J. Hu, *Phys. Rev. B*, 2017, **96**, 174506.